Received: 13 June 2023 | Revised: 23 April 2024 | Accepted: 24 April 2024

DOI: 10.1111/apha.14160

ACTA PHYSIOLOGICA

RESEARCH PAPER

Striatin knock out induces a gain of function of I_{Na} and impaired Ca^{2+} handling in mESC-derived cardiomyocytes

P. Benzoni[1] | M. Arici[2] | F. Giannetti[1] | A. Cospito[1] | R. Prevostini[1] | C. Volani[1,3] | L. Fassina[4] | M. D. Rosato-Siri[3] | A. Metallo[2] | L. Gennaccaro[3] | S. Suffredini[3] | L. Foco[3] | S. Mazzetti[5] | A. Calogero[5] | G. Cappelletti[5] | A. Leibbrandt[6] | U. Elling[6] | F. Broso[3] | J. M. Penninger[6,7] | P. P. Pramstaller[3] | C. Piubelli[3] | A. Bucchi[1] | M. Baruscotti[1] | A. Rossini[3] | M. Rocchetti[2] | A. Barbuti[1]

[1]Department of Biosciences, The Cell Physiology MiLab, Università Degli Studi Di Milano, Milan, Italy

[2]Department of Biotecnologie e Bioscienze, Università degli Studi di Milano Bicocca Milano, Milan, Italy

[3]Institute for Biomedicine, Eurac Research, Bolzano, Italy

[4]Department of Electrical, Computer and Biomedical Engineering, University of Pavia, Pavia, Italy

[5]Department of Biosciences, Università Degli Studi Di Milano, Milan, Italy

[6]IMBA, Institute of Molecular Biotechnology of the Austrian Academy of Sciences, Vienna, Austria

[7]Department of Medical Genetics, The University of British Columbia, Vancouver, British Columbia, Canada

Correspondence

A. Barbuti and P. Benzoni, Department of Biosciences, The Cell Physiology MiLab, Università Degli Studi Di Milano, Milan, Italy.
Email: andrea.barbuti@unimi.it and patrizia.benzoni@unimi.it

Present addresses

F. Giannetti, Istituto Auxologico Italiano IRCCS, Center for Cardiac Arrhythmias of Genetic Origin and Laboratory of Cardiovascular Genetics, Milano, Italy

R. Prevostini, MTC—Institute of Molecular and Translational Cardiology, San Donato Milanese

L. Gennaccaro, Center for Synaptic Neuroscience and Technology (NSYN), Italian Institute of Technology (IIT), Genova, Italy

F. Broso, Laboratory of Translational Genomics, Department of Cellular, Computational and Integrative Biology, University of Trento, Trento, Italy

C. Piubelli, Department of Infectious, Tropical Diseases and Microbiology, IRCCS Sacro Cuore Don Calabria Hospital, Negrar, Italy

Funding information

Department of Innovation, Research and University of the Autonomous Province of Bolzano, Italy, through a core funding initiative to the Eurac Institute for Biomedicine; This work

Abstract

Aim: Striatin (Strn) is a scaffold protein expressed in cardiomyocytes (CMs) and alteration of its expression are described in various cardiac diseases. However, the alteration underlying its pathogenicity have been poorly investigated.

P. Benzoni and M. Arici equally contributed to the work as first authors.

M. Rocchetti and A. Barbuti equally contributed to the work as last authors.

was also supported by the Universities of Milano and Milano Bicocca

Methods: We studied the role(s) of cardiac Strn gene (*STRN*) by comparing the functional properties of CMs, generated from Strn-KO and isogenic WT mouse embryonic stem cell lines.

Results: The spontaneous beating rate of Strn-KO CMs was faster than WT cells, and this correlated with a larger fast I_{Na} conductance and no changes in I_f. Paced (2–8 Hz) Strn-KO CMs showed prolonged action potential (AP) duration in comparison with WT CMs and this was not associated with changes in I_{CaL} and I_{Kr}. Motion video tracking analysis highlighted an altered contraction in Strn-KO CMs; this was associated with a global increase in intracellular Ca^{2+}, caused by an enhanced late Na^+ current density (I_{NaL}) and a reduced Na^+/Ca^{2+} exchanger (NCX) activity and expression. Immunofluorescence analysis confirmed the higher Na^+ channel expression and a more dynamic microtubule network in Strn-KO CMs than in WT. Indeed, incubation of Strn-KO CMs with the microtubule stabilizer taxol, induced a rescue (downregulation) of I_{Na} conductance toward WT levels.

Conclusion: Loss of *STRN* alters CMs electrical and contractile profiles and affects cell functionality by a disarrangement of Strn-related multi-protein complexes. This leads to impaired microtubules dynamics and Na^+ channels trafficking to the plasma membrane, causing a global Na^+ and Ca^{2+} enhancement.

KEYWORDS

arrhythmias, calcium, microtubules, sodium current, Striatin

1 | INTRODUCTION

Striatin (Strn) is a 86 kDa scaffolding protein, composed of 780 amino acids, characterized by four protein–protein interaction domains: (i) a caveolin-binding domain, (ii) a coiled–coiled structure essential for oligomerization, (iii) a Ca^{2+}-calmodulin binding domain that function as a Ca^{2+} sensor, and (iv) a tryptophan-aspartic acid repeat domain involved in multiple protein–protein interactions.[1–3] Strn and other related members of its family (i.e., S/G2 nuclear autoantigen and Zinedin) were originally discovered in the brain and more precisely in the striatum, but were then found almost ubiquitously expressed (as reported in the Human Protein Atlas http://www.proteinatlas.org/ENSG00000115808-STRN/tissue). Recently, some cardiovascular diseases have been associated with genetic variants in the Strn gene (*STRN*). A genome-wide association study (GWAS) on arrhythmogenic right ventricular cardiomyopathy (ARVC) in boxer dogs identified a deletion of eight base pairs in the 3′ untranslated region of *STRN*. This deletion caused a reduction in the expression of Strn mRNA, due to alteration of the secondary structure that decreased its stability.[4] In another study, the same *STRN* mutation was associated with the development of canine dilated cardiomyopathy (DCM), characterized by a dysfunction and dilatation of both left and right ventricle.[5] In humans, a GWAS study associated the locus of *STRN* with changes in the QRS complex duration.[6] This finding was recently confirmed in a genome-wide association meta-analysis where *STRN* has been identified among 52 independent loci displaying a significant association with QRS duration.[7] In the same work, a RNA interference knockdown of *STRN* triggered cardiac defects in the heart of adult *Drosophila melanogaster*. Altogether, these studies suggest that Strn could be an interesting novel candidate for the pathogenesis of cardiovascular diseases.

The present work investigated how the lack of Strn affects the functional properties of cardiomyocytes (CMs) derived from mouse Strn-knockout (Strn-KO) Embryonic Stem Cells (mESC).

We provide evidence that Strn-KO CMs obtained by spontaneous differentiation through the generation of embryoid bodies (EBs), displayed dysregulation in contraction and intracellular Ca^{2+} handling, beating rate and action potential (AP) onset and duration, mainly related to the increase of transient and late sodium current (I_{Na}) density. We suggest a dysregulated cytoskeletal network/ion channel function, as the causative reason for Strn-KO-induced changes.

Overall, these results provide the first mechanistic evidence that the lack of Strn significantly alters both the electrical and mechanical properties of CMs, opening the

pathways to novel therapies for cardiac diseases and contractile dysfunction.

2 | RESULTS

2.1 | Evaluation of cardiac gene expression

Strn-KO cells were tested for their ability to differentiate toward the cardiomyogenic fate. To this aim, we evaluated the expression of cardiac genes after 12 days of differentiation. No differences were found between Strn-KO and WT (Table S2).

2.2 | Strn expression

Strn mRNA expression was confirmed to be significantly down-modulated in Strn-KO versus WT (Table S2). Moreover, Strn protein expression was also assessed by western blot (Figure S2). Samples were collected at Day 0 (undifferentiated mESCs) and in beating EBs at Days 12 and 20 of differentiation. Adult murine cardiac tissue was used as positive control. While the presence of Strn was evident in both WT mESCs and EBs, and in the mouse heart, the protein was only slightly detectable in Strn-KO mESC and EBs.

2.3 | Contractile activity

Motility features of beating areas of the EBs were analyzed by Video Spot Tracker (VST) and a custom-made algorithm.[8] This analysis detected, along with a normal contraction pattern (Figure 1A), "non-complete" or "short and abortive" contractions (Figure 1B) in both WT and Strn-KO EBs. While the frequency of normal contractions tended to be reduced (Strn-KO: 0.64 ± 0.08 Hz, $N = 19$; WT: 0.80 ± 0.18 Hz, $N = 7$, NS), the incidence of abortive events was significantly higher in Strn-KO than in WT EBs (72% vs. 22% respectively,

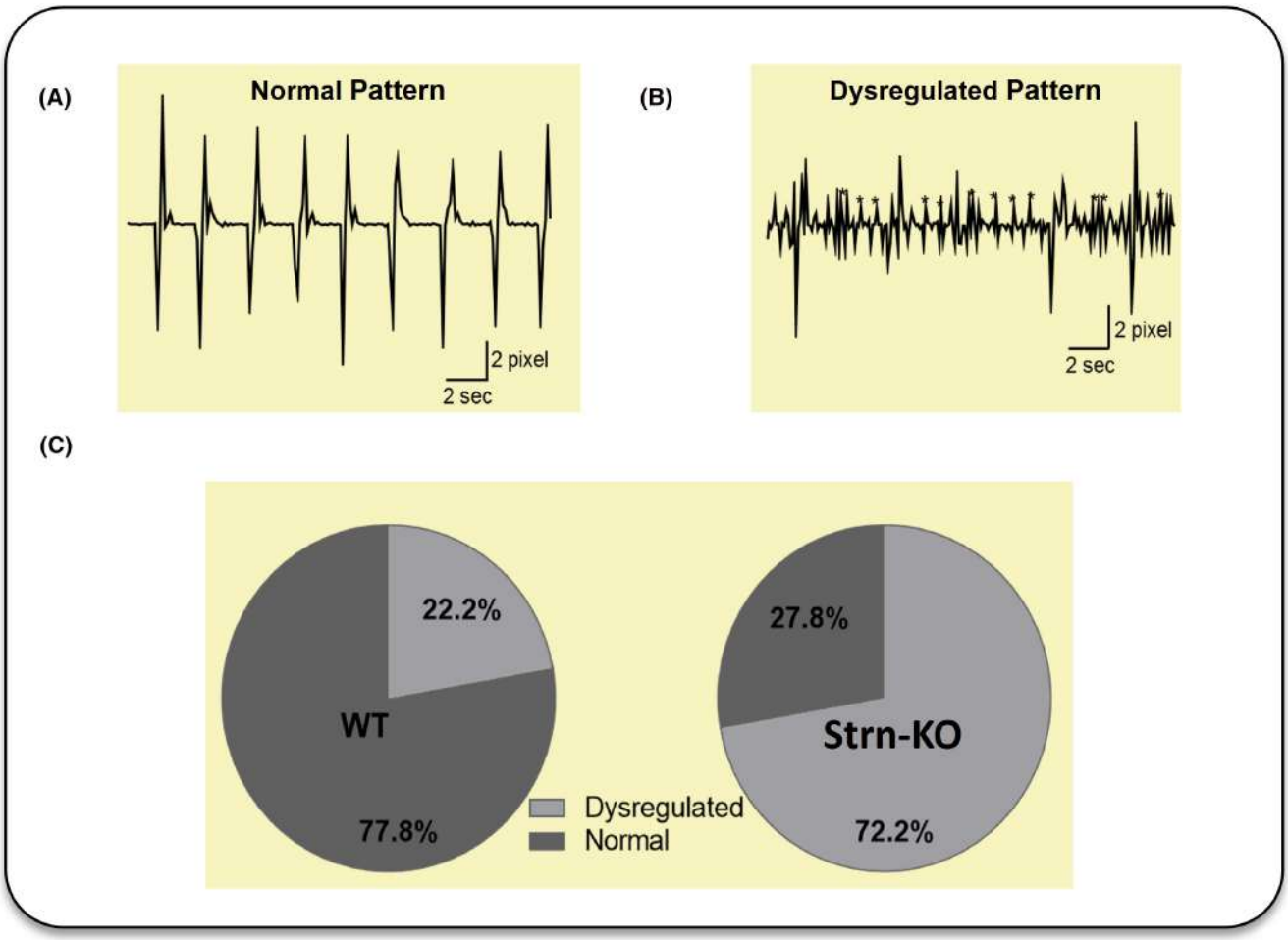

FIGURE 1 Representative traces showing normal (A) and dysregulated (B) contractions occurring in both WT and Strn-KO beating aggregates (VST analysis, where the amplitude is the extent of pixel movement). (C), pie charts showing the different proportion of dysregulated contractions in WT (left, $N = 19$ beating area) versus Strn-KO (right, $N = 19$ beating area) aggregates.

Figure 1C), suggesting that an abnormal contraction activity is associated with the lack of Strn expression.

2.4 | Electrical activity

To better understand the anomalies in Strn-KO contractions, we assessed the electrical properties of CMs enzymatically isolated from beating areas of both groups. Firstly, we recorded APs from spontaneously beating cells. Strn-KO CMs showed a higher beating rate (representative traces in Figure 2A) compared with WT CMs. Mean rate values were 3.9 ± 0.3 Hz and 5.5 ± 0.6 Hz for WT and Strn-KO ($p < 0.05$), respectively (Figure 2B).

Moreover, the slope of the fast depolarization phase (dV/dt_{max}, Figure 2B) was significantly faster in Strn-KO (12.8 ± 1.6 V/s) than in WT (7.5 ± 1.0 V/s) CMs. No differences were observed for the other AP parameters (Figure 2B), namely the AP amplitude (APA), the maximum diastolic potential (MDP) and the duration at 50 and 90% of repolarization (APD_{50} and APD_{90}).

Since the APD is dependent on AP rate, we also analyzed the AP parameters in paced CMs at 2 Hz (Figure 3A,B). In comparison with WT CMs, Strn-KO CMs showed prolonged APD_{50} (Strn-KO 53.13 ± 5.31 ms vs. WT 36.85 ± 5.88 ms, $p < 0.05$) and APD_{90} (Strn-KO 76.48 ± 7.06 ms vs. WT 52.96 ± 6.84 ms, $p < 0.05$), without changes in diastolic potential (E_{diast}) and amplitude (APA).

In order to overcome the partially depolarized membrane potential of these cells (Figure 3B), APs were elicited by injecting a numerical I_{K1} using the DC technique (see Section 4) and the rate dependency (2–8 Hz) of AP parameters was examined (Figure 3C–E). Strn-KO CMs exhibited longer APD than WT CMs, especially at low pacing rates. The short-term variability (STV) of APD_{90}, a reporter of repolarization instability, similarly correlated with APD_{90} values measured at all pacing rates in the two groups (Figure 3E), suggesting that APD prolongation in Strn-KO cells is per se a determinant factor of a proarrhythmic phenotype in these cells. Finally, the incidence of delayed after depolarizations (DADs) was not statistically different in the two experimental groups.

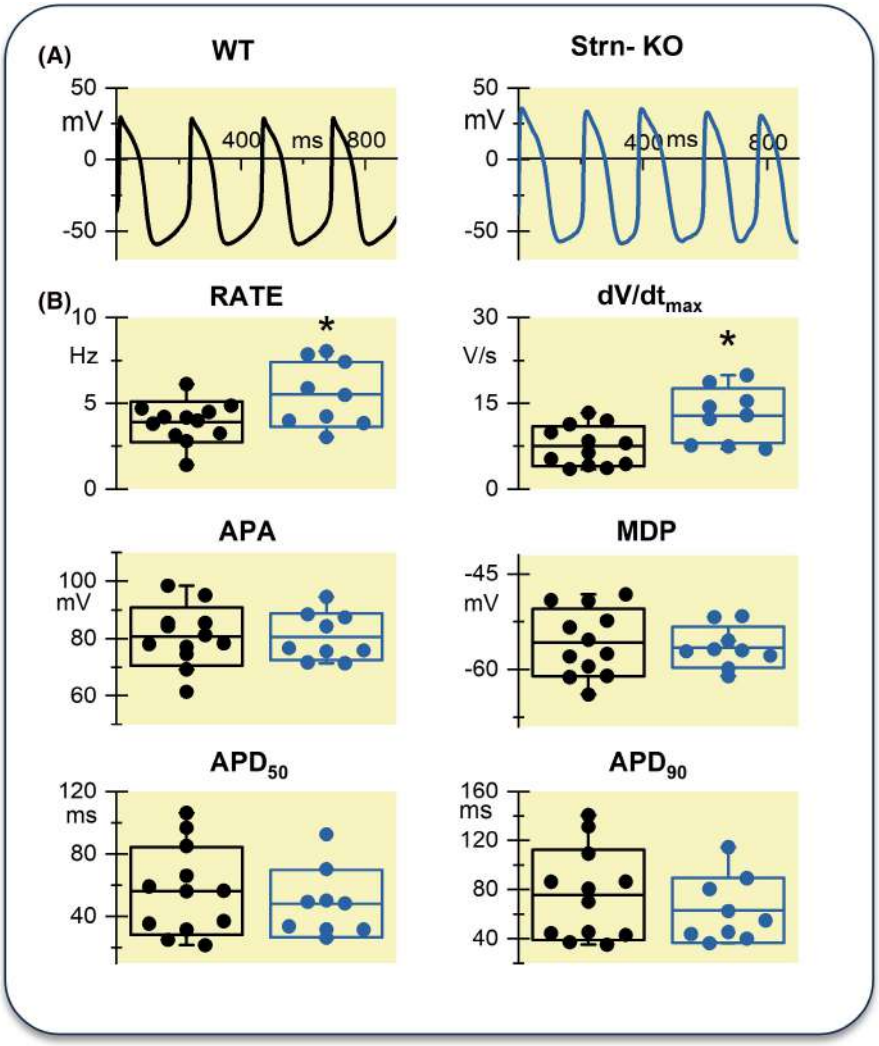

FIGURE 2 (A) Representative spontaneous AP traces recorded from isolated WT (black) and Strn-KO (blue) CMs. (B) Dot plots of the analyzed AP parameters: rate, maximal steepness of fast depolarization (dV/dt_{max},); AP amplitude (APA): maximum diastolic potential (MDP); AP duration at 50% and 90% of repolarization (APD_{50} and APD_{90}); colors as in A. WT: $N = 11$, KO: $N = 9$. *$p < 0.05$ versus WT.

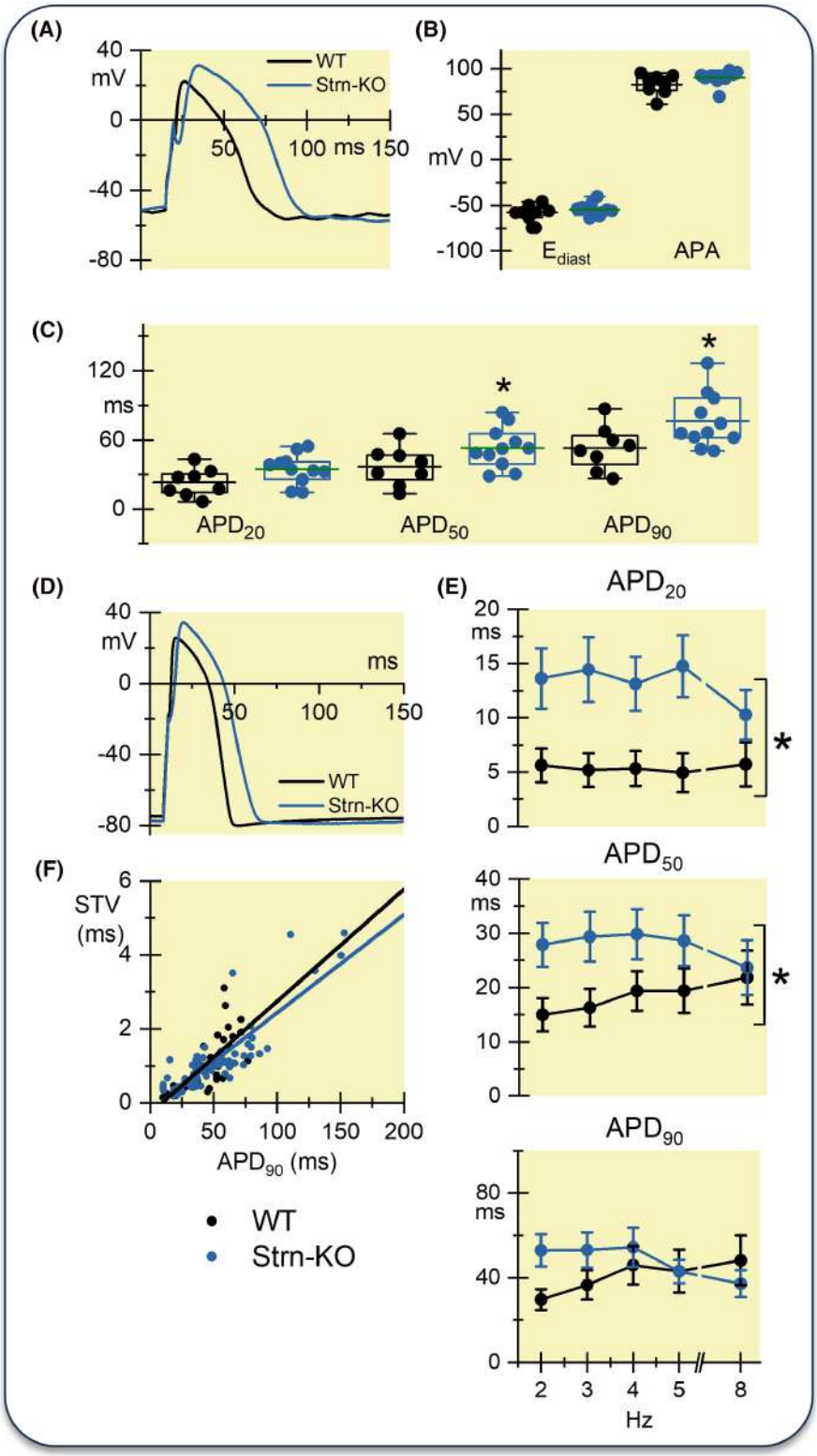

FIGURE 3 (A) Representative AP traces evocated at 2 Hz in isolated WT (black) and Strn-KO (blue) CMs. (B, C) Dot plots of the analyzed AP parameters (color as in A): diastolic membrane potential (E_{diast}), AP amplitude (APA), and AP duration at 20, 50, and 90% of repolarization (APD_{20}, APD_{50}, and APD_{90}). WT: $N = 9$, KO: $N = 11$. *$p < 0.05$ versus WT. (D) Representative APs recorded at 2 Hz under DC technique by injecting numerical I_{K1} (see Methods). (E) rate dependency of AP parameters (APD_{20}, APD_{50}, APD_{90}) in WT ($N = 5$–12) and Strn-KO ($N = 10$–21) CMs (color as in A). *$p < 0.05$ versus WT (two-way ANOVA). (F) Linear correlations between short-term variability (STV) of APD_{90} and the corresponding APD_{90} values in both groups (data from all stimulation rates were pooled).

2.5 | Ionic currents

To investigate the mechanisms explaining the alterations observed in Strn-KO cells, we evaluated the main ionic currents underlying specific AP phases. Because of the known role of $Na_V1.5$ in spontaneously beating ESC-derived CMs, in sinus node firing rate, and in setting the dV/dt_{max} of the AP,[9,10] we first analyzed the fast sodium current (I_{Na}). Figure 4A shows representative TTX-sensitive I_{Na} traces recorded in WT and Strn-KO CMs (see also Figure S3A). I-V relations plotted in panel B show a significantly larger maximal Na^+ conductance in Strn-KO (2.7 ± 0.5 nS/pF) than in WT (1.4 ± 0.2 nS/pF) CMs. I_{Na} steady-state activation and inactivation curves were instead unaffected (panel C). The

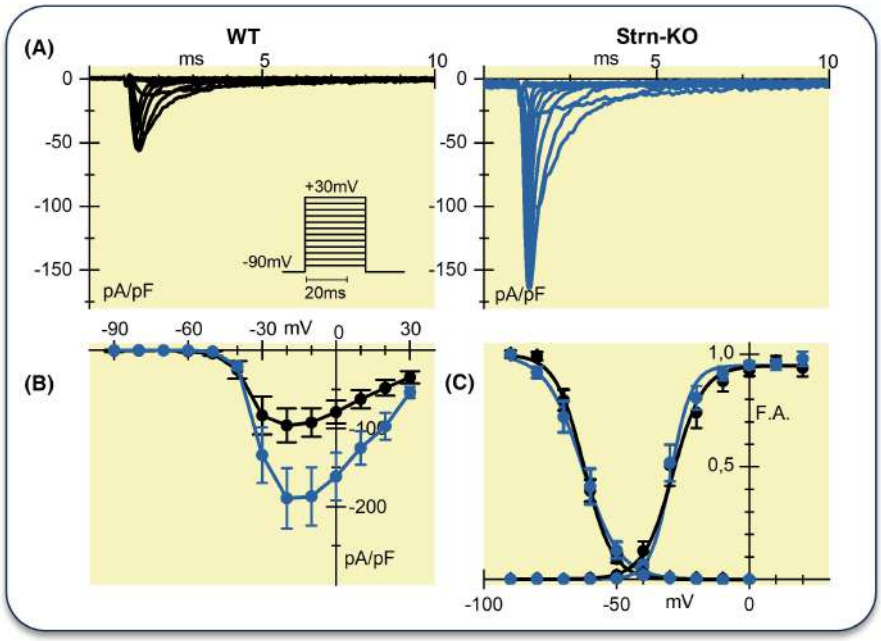

FIGURE 4 (A) Representative I_{Na} traces recorded in isolated WT (black) and Strn-KO (blue) CMs according to the voltage protocol in the inset. (B) Mean I-V relations of I_{Na} in WT (black circles, $N=13$) and Strn-KO (blue circles, $N=14$) cells. (C) Mean activation and inactivation curves of I_{Na} (colors as in A, B).

increased expression of $Na_V1.5$ in Strn-KO CMs was further confirmed by immunofluorescence analysis (Figure S4 for representative images). To notice, SCN5A transcript level was comparable in Strn-KO and WT CMs (Table S2).

The increase in spontaneous AP rate in Strn-KO cells was not associated with changes in the pacemaker I_f current (Figure S5A); no differences were found either in current densities or in kinetics between Strn-KO and WT cells. Moreover, the increased velocity of the AP phase 0 in Strn-KO cells was not associated with changes in I_{CaL}. Figure S5B shows representative traces of 10 μM nifedipine-sensitive I_{CaL} recorded from WT and for Strn-KO CMs (see also Figure S3B); no alterations were found neither in current density nor in activation/inactivation kinetics between WT and Strn-KO cells. To notice, HCN (1, 2, 4) and CACNA1C transcript levels were comparable in Strn-KO and WT CMs (Table S2). Finally, the rapid delayed rectifier K^+ current (I_{Kr}, Figure S5C) was not affected in Strn-KO cells neither in terms of conductance nor in kinetics (see also Figure S3C).

Overall, these data suggest that the increase in AP firing rate in Strn-KO cells was likely caused by a gain of function of functional Na^+ channels, while changes in APD were not dependent on changes in I_{CaL} and I_{Kr}.

2.6 | Intracellular Ca^{2+} and Na^+ dynamics

To further characterize the Strn-KO phenotype and explain contractile anomalies, we investigated the intracellular Ca^{2+} dynamics. To measure direct effects of Strn on intracellular Ca^{2+} levels and avoid secondary changes related to changes in firing rate, Ca^{2+} transients (CaT) were evocated in Fluo4 voltage-clamped CMs. Resting Ca^{2+} (Ca_{rest}), CaT amplitude and sarcoplasmic reticulum Ca^{2+} content (Ca_{SR}), evaluated through a caffeine (10 mM) pulse, were significantly larger in Strn-KO CMs (Figure 5A,B) in comparison with WT.

Moreover, to estimate changes in the NCX activity, the correlation between the NCX current (I_{NCX}) and the cytosolic Ca^{2+} levels (Figure 5C) during caffeine superfusion was analyzed. In Strn-KO CMs, the linear correlation was less steep (reduced slope) and shifted to the right (increased Ca_{eq}), suggesting a reduction in the rate of Ca^{2+} extrusion through NCX at resting membrane potential (−80 mV), thus justifying the increased cytosolic Ca^{2+} in Strn-KO CMs. Otherwise, the increased Ca_{SR} in Strn-KO CMs was not associated with changes in SERCA2a transcript (Table S2) and protein levels (Figure S6).

Since NCX is known to be dependent on Na^+ gradient, we postulated a sustained increase in intracellular Na^+ levels via the late component of I_{Na} (I_{NaL}) to explain its reduced activity and the related global cytosolic Ca^{2+} enhancement in Strn-KO cells. I_{NaL} was evaluated as the steady-state TTX (2 μM)-sensitive current (I_{TTX}) activated at −20 mV by applying slow voltage ramps (Figure 6A,B).[11] I_{NaL} significantly increased in Strn-KO compared with WT (−0.34 ± 0.04 pA/pF vs. −0.15 ± 0.04 pA/pF, $p<0.05$); the peak I_{TTX} activated at negative potentials (mostly representing the Na^+ window current) was unaltered in Strn-KO cells, accordingly to unchanged steady-state activation and inactivation curves of transient I_{Na} (see Figure 4C).

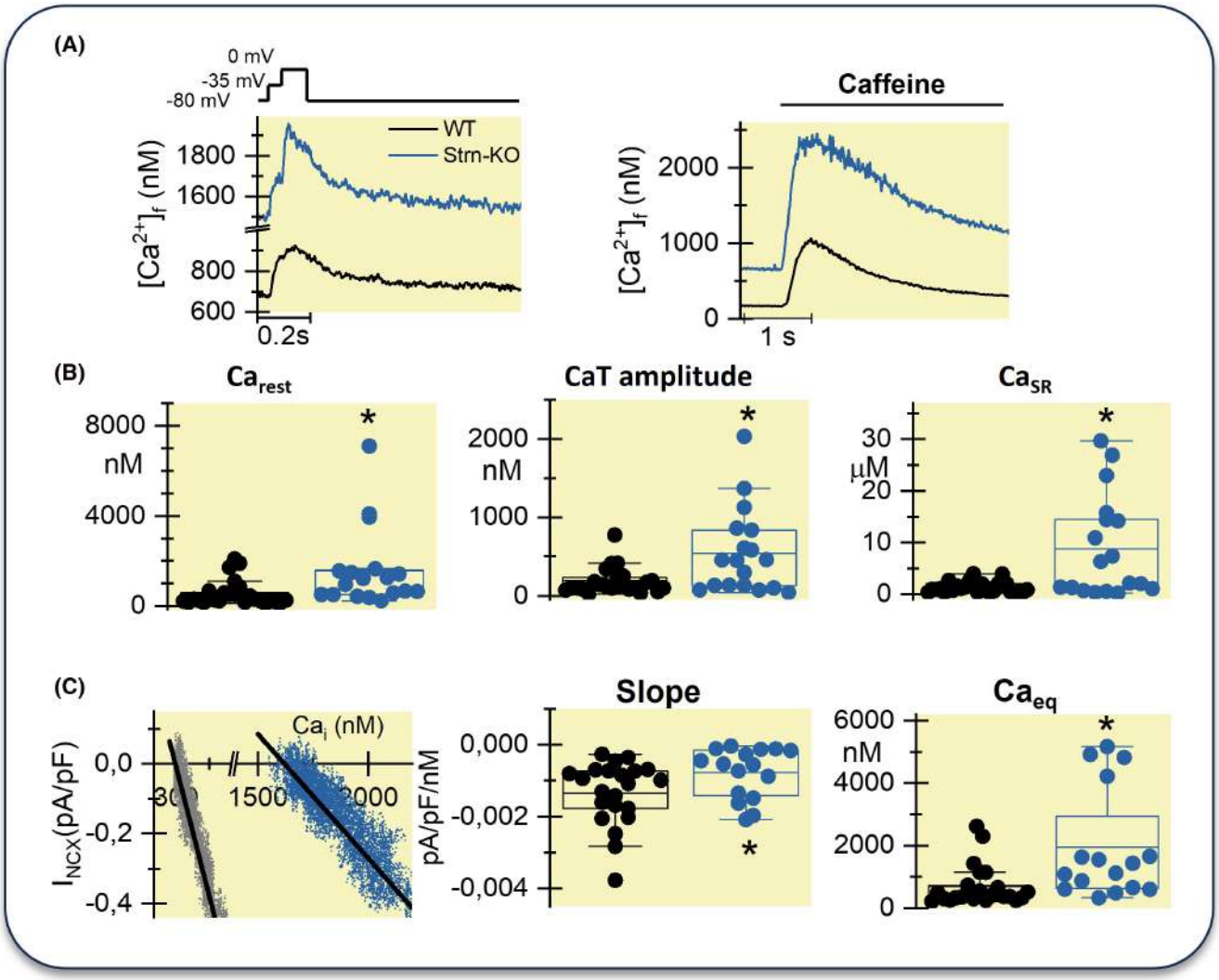

FIGURE 5 (A) Representative voltage- (left) and caffeine-(right) induced Ca^{2+} transients (CaT) recorded in Fluo4-loaded WT (black) and Strn-KO (blue) CMs. (B) statistics of resting Ca^{2+} (Ca_{rest}), CaT amplitude and SR Ca^{2+} content (Ca_{SR}) levels in WT ($N = 25$, black circles) and Strn-KO ($N = 18$, blue) CMs; $* = p < 0.05$ versus WT. (C) linear correlation (left) between NCX current (I_{NCX}) and Ca_i during the third part of the caffeine-induced CaT, and statistics of the slope (middle) and x-axis intercept (Ca_{eq}, right) in WT ($N = 22$, black) and Strn-KO ($N = 16$, blue) CMs. $* = p < 0.05$ versus WT.

To further confirm the altered ionic homeostasis in Strn-KO CMs, cytosolic Na^+ levels (Na_i) were measured in both groups by using the Na^+-sensitive dye SBFI in a cell population analysis. As expected, Na_i resulted significantly higher in Strn-KO CMs than in WT (Figure 6C).

These findings suggest that the primary cause of intracellular Ca^{2+} enhancement in Strn-KO CMs was a reduced Na^+ gradient and a consequent drop in NCX working activity. Moreover, I_{NCX} measured in the absence of intracellular Na^+ and Ca^{2+} oscillations (Figure 6D) was reduced in Strn-KO CMs compared to WT, at both negative (normal mode working condition) and positive (reverse mode working condition) potentials, suggesting that reduced NCX expression in Strn-KO cells can further explain the increased Ca^{2+} level in these cells.

2.7 | Microtubule dynamics and rescue of the I_{Na}

The known inhibitory effect of microtubule dynamics on $Na_v1.5$ current density following the use of the anticancer tubulin-stabilizing drug taxol[12] together with the known role of Strn downregulation on cytoskeleton[13] brought us to hypothesize that Strn may be at least the link between microtubules dynamics and $Na_v1.5$ channel trafficking. This prompted us to investigate whether stabilization of microtubules with taxol could rescue the gain of function of I_{Na} observed in Strn-KO CMs.

Figure 7 shows representative images of WT and Strn-KO CMs stained with anti-troponin (green), anti-total tubulin (white) and either the anti-tyrosinated (red, top panels) or

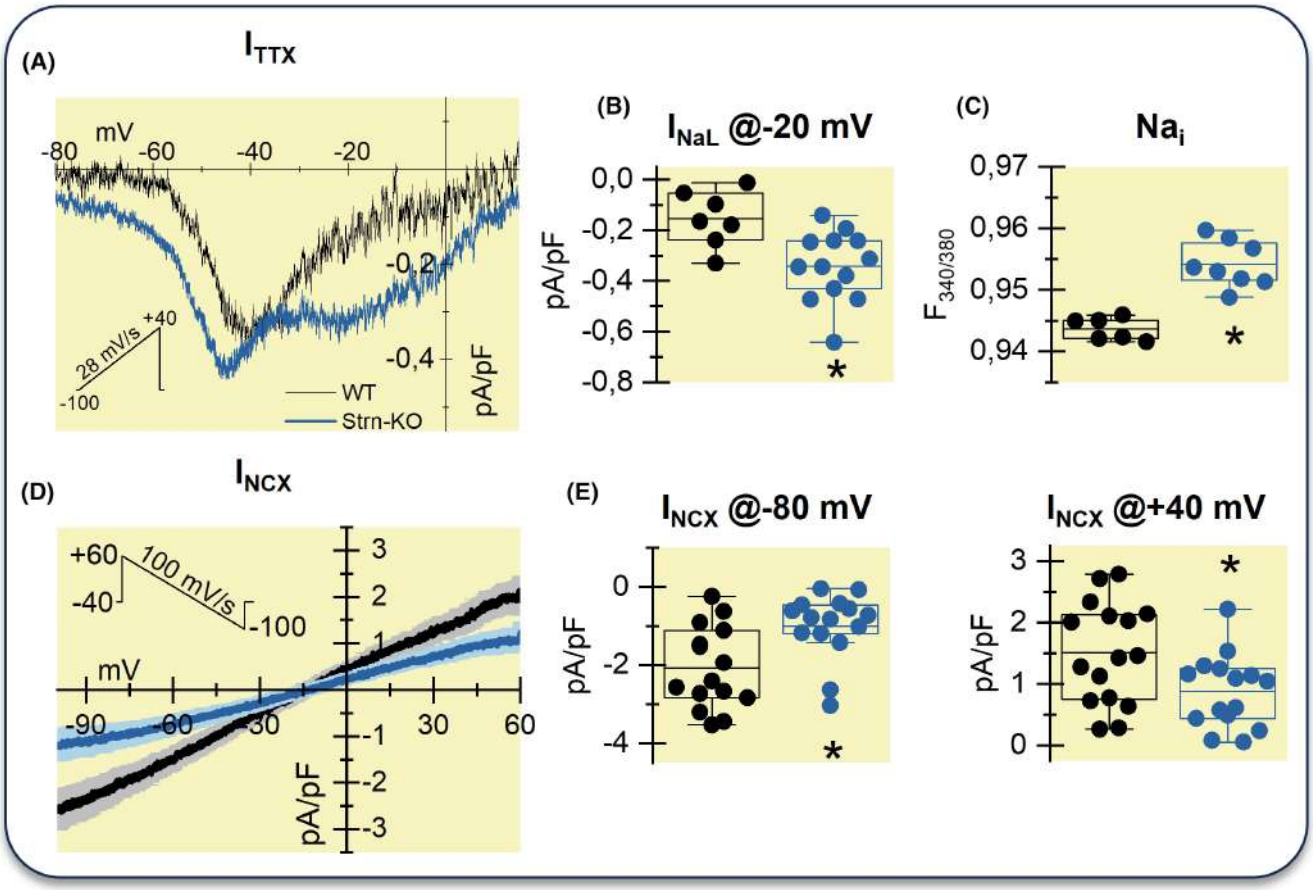

FIGURE 6 (A) Mean I-V relations (left) of TTX-sensitive current (I_{TTX}) in WT ($N=7$, black line) and Strn-KO ($N=13$, blue line) CMs, according to the voltage protocol in the inset. (B) statistics of I_{TTX} measured @ -20 mV, largely representing I_{NaL}; $*=p<0.05$ versus WT. (C) Intracellular Na^+ level (Na_i) in (5 μM) SBFI loaded WT ($N=6$; black) and Strn-KO ($N=8$; blue) cells (population analysis). $*=p<0.05$ versus WT. (D) Mean I-V relations of NCX current (I_{NCX}) in WT ($N=16$, black line) and Strn-KO ($N=15$, blue line) CMs, according to the voltage protocol in the inset. (E) Statistics of I_{NCX} measured @ −80 mV (left) and @ +40 mV (right), largely representing the forward and the reverse mode working direction of NCX, respectively. $*=p<0.05$ versus WT.

anti-acetylated (red, bottom panels) tubulin antibodies. Strn-KO cells showed more tyrosinated (Figure 7C) and less acetylated (Figure 7D) tubulin than WT cells. This evidence suggests a more dynamic tubulin network in Strn-KO CMs than in WT. Moreover, total α-tubulin protein expression level was reduced in Strn-KO cells (Figure S6C).

To study whether the I_{Na} difference may be ascribed to differences in tubulin dynamics, we treated WT and Strn-KO CMs with either taxol (10 μM paclitaxel) or vehicle (DMSO) for 4 h before recording I_{Na}. As shown in Figure 8, taxol did not alter I_{Na} conductance in WT CMs (DMSO 1.5 ± 0.3 pS/pF; taxol 1.6 ± 0.3 pS/pF, NS), while it significantly decreased I_{Na} conductance in Strn-KO cells from 3.0 ± 0.6 pS/pF in DMSO to 0.9 ± 0.1 pS/pF in taxol.

3 | DISCUSSION

In the present work, using mESC we demonstrated that the lack of the *STRN* gene, leads to significant alterations of CMs function, both at the level of contractility and electrophysiological properties.

The video analysis of contraction demonstrated a higher incidence of "abortive events" when the excised EBs' beating areas were analyzed from spontaneously beating Strn-KO CMs aggregates.

Notably, while frequency of normal contractions was not significantly changed, when we evaluated the spontaneous AP firing in isolated CMs, we observed an increased AP frequency in Strn-KO respect to the WT. This suggests that abortive contractions might derive from an altered excitation contraction coupling machinery. The higher beating frequency could simply reflect an immature stage of Strn-KO CMs compared to WT, even though this seems unlikely given the lack of differences in the other parameters of spontaneous AP. Of note, although the role of the pacemaker I_f current in setting the spontaneous activity of pluripotent stem cell-derived beating CMs is well known,[14–16] the I_f current amplitude and kinetic properties did not change in Strn-KO cells. On the contrary, the

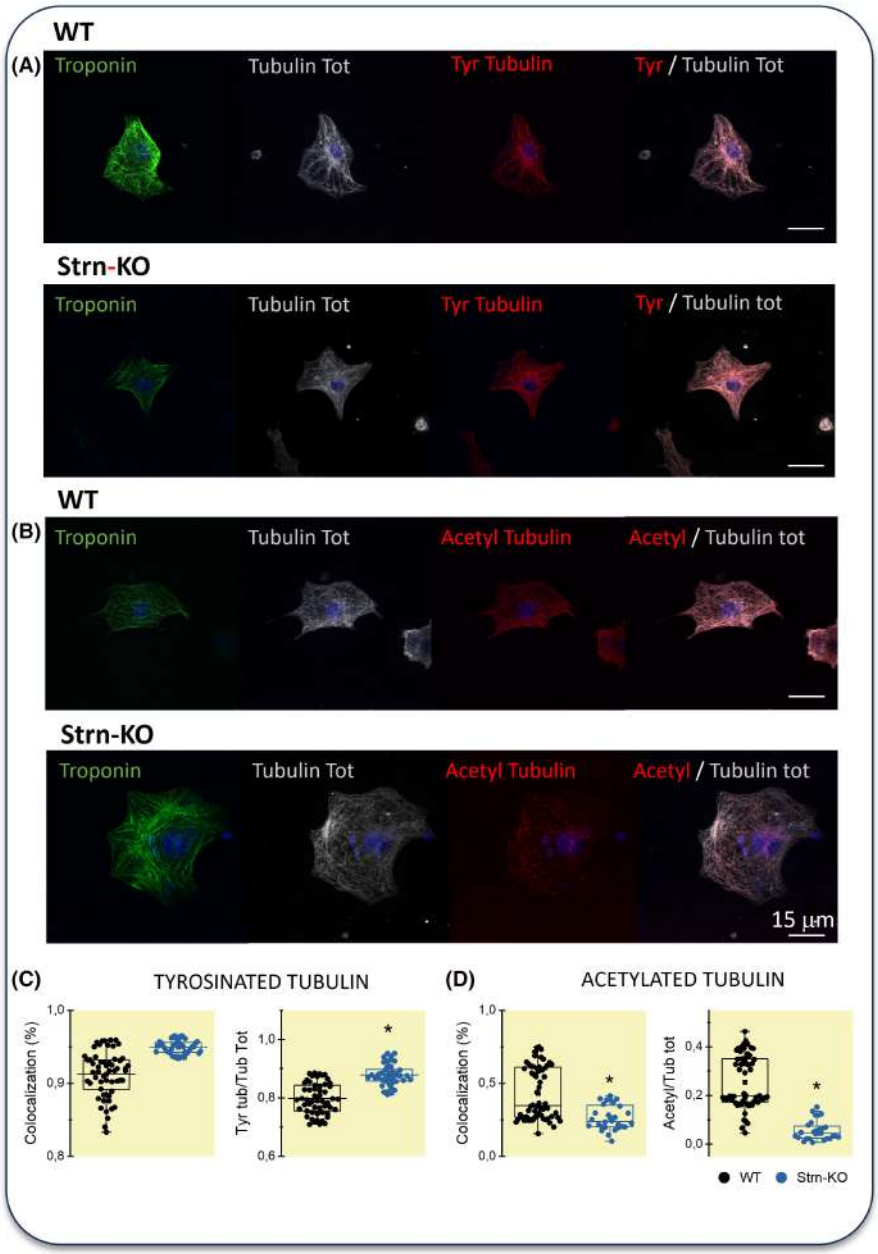

FIGURE 7 (A) representative immunofluorescence images of troponin$^+$ (green) WT and Strn-KO CMs labeled with anti-total-tubulin (white) and anti-tyrosinated (red) tubulin Abs. (B) representative immunofluorescence images of troponin$^+$ (green) WT and Strn-KO CMs labeled with anti-total-tubulin (white) and anti-acetylated (red) tubulin Abs. Far rights images are the merged images of total and either tyrosinated or acetylated tubulin. Nuclei were counterstained with dapi (blue). Calibration bar = 15 µm. (C) dot plots of Pearson (left) and Manders (right) coefficients that indicate the colocalization of the tyrosinated and total tubulin and how much of the total tubulin is tyrosinated in WT (black) and Strn-KO (blue), respectively. (D) dot plots of Pearson (left) and Manders (right) coefficients measured in WT (black dots) and Strn-KO (blue dots) that indicate the colocalization of the acetylated and total tubulin and how much of the total tubulin is acetylated, respectively. (WT: $N = 60$ slices/6; KO: $N = 54$ slices/5). *$p < 0.05$ versus WT.

fast I_{Na} largely increased, thus well explaining the higher beating rate of Strn-KO cells.[17]

Moreover, in Strn-KO CMs APD resulted prolonged when evaluated under stimulated AP, thus suggesting changes in inward and/or outward currents activated during the repolarization phase. In Strn-KO cells both L-type Ca^{2+} current (I_{CaL}) and the delayed rectifier K^+ current (I_{Kr}) were not significantly altered. However, the late component of I_{Na} (I_{NaL}) increased in Strn-KO cells. This well supports the prolonged APD in particular at low pacing rates, in agreement with the use dependency of I_{NaL}.[18] It is well known that I_{NaL} enhancement occurs in many pathological conditions and can profoundly alter intracellular ionic homeostasis with consequences on contractile function, electrical stability, and cell fate.[18]

Thus, increased I_{NaL} in Strn-KO cells might largely explain the altered contractility of these cells. The search of a mechanism inducing I_{NaL} enhancement has highlighted the role of Ca^{2+}-calmodulin kinase (CaMKIIδ) activation,[19] particularly relevant because its relation with I_{NaL} may set up a vicious feedback loop very likely to contribute to evolution of cell dysfunction and damage. Strn is a dynamic protein with binding domains to calmodulin and caveolin; thus, a hypothetical dysregulated calmodulin/CAMKII activity in Strn-KO cells might explain the observed alterations in I_{Na} properties.

NCX is the main mechanism of Ca^{2+} extrusion from the cell. Increased cytosolic Na^+ due to I_{NaL} enhancement moves its electrochemical equilibrium potential in the negative direction, thus reducing the driving force for its

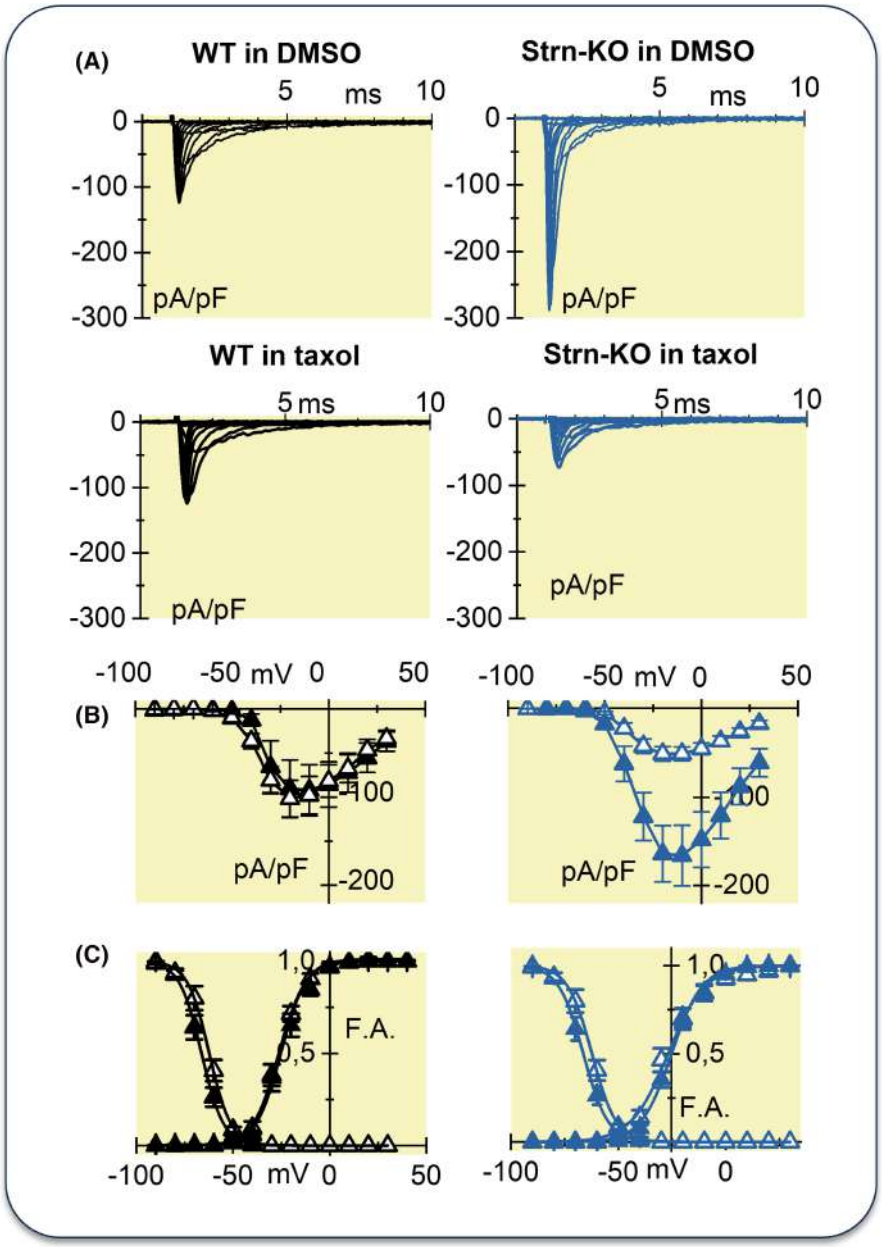

FIGURE 8 (A) Representative I_{Na} traces recorded from isolated WT (black) and Strn-KO (blue) CMs incubated for 4 h with either DMSO (vehicle, top) or with Paclitaxel (taxol) dissolved in DMSO (bottom). (B) Left, mean I-V relations of I_{Na} analyzed from DMSO-treated (black triangles) and taxol-treated WT cells (empty black triangles) WT: $N = 7$ KO: $N = 8$. (B) Right, mean I-V relations of I_{Na} analyzed from DMSO-treated (blue triangles) and taxol-treated Strn-KO cells (empty blue triangles) WT: $N = 11$, KO: $N = 14$. (C) Mean activation and inactivation curves of WT and Strn-KO Na^+ channels (symbols and colors as in B).

forward operation during diastole. Thus, an increase in total cellular Ca^{2+} content is a necessary consequence of I_{NaL} enhancement. Accordingly, Strn-KO CMs showed a global cytosolic Na_i and Ca^{2+} enhancement, in terms of increased resting Ca^{2+} and SR Ca^{2+} content. This was linked to decreased NCX activity for both altered protein expression and Na^+/Ca^{2+} homeostasis.

Importantly, Strn acting as scaffolding protein takes part in the assembly of Striatin-interacting phosphatase and kinase (STRIPAK) complexes.[20] Within STRIPAK, Strn has been shown to interact with the component SLMAP (tail-anchored membrane protein). This has cardiac muscle-specific isoforms and was hypothesized to play a role in the EC-coupling machinery[21] both impacting SR structure and the expression of SR Ca^{2+}-handling proteins.[22]

Moreover, cardiac Na^+ channels were previously associated with the microtubules dynamics, indeed Casini et al[12] demonstrated that both HEK 293 cells transfected with $Na_V1.5$ and the native channel in neonatal CMs express a smaller I_{Na} when treated with the microtubules stabilizing drug taxol. Our data show that Strn-KO CMs expressed a larger I_{Na} than WT, suggesting that somehow the microtubule dynamics might be altered in the absence of Strn. This hypothesis has been confirmed by treating Strn-KO CMs with taxol, which induced a significant reduction of I_{Na} to levels comparable to those of WT CMs, suggesting a more dynamic microtubules network in KO cells.

To evaluate the role of cytoskeleton and in particular of microtubules in Na^+ channel trafficking, we measured the expression of total, the acetylated and tyrosinated

forms of tubulin in both WT and Strn-KO CMs. While acetylated tubulin is indicative of microtubules more resistant to breakage following mechanical stress,[23] tyrosination globally reduces microtubule stability.[24] Our results (Figure 7) show that Strn-KO cells have more tyrosinated tubulin/total tubulin ratio than WT CMs and less acetylated tubulin/total tubulin ratio. Interestingly, drugs decreasing the microtubule stability (colchicine) induce an increased I_{Na}, a faster beating rate and a larger AP dV/dt_{max}, without alteration of Ca^{2+} current.[25] These effects were well reproduced in our Strn-KO CMs. The less acetylated tubulin in Strn-KO CMs, is indicative of microtubules less resistant to breakage following mechanical stress. We can speculate that this altered microtubules network may contribute to the higher "abortive" contraction rate observed in Strn-KO CMs, compared to WT CMs. Notably, in vitro studies have shown that DCM-associated $Na_v1.5$ variants have either loss-of-function or gain-of-function effects on Na^+ channel[26] thus indicating that molecular mechanisms responsible for $Na_v1.5$-related cardiomyopathy are rather multifaceted and not fully yet explored. Our study underlying the relevance of Strn effect on cardiac function can contribute to shed some light in this complex field.

Importantly, our findings do not show a different expression of cardiac genes between WT and Strn-KO, thus indicating a relative homogeneity between the two lines and further sustaining the view that the loss of Strn may affect cardiac function not through a transcriptional mechanism, but by causing the disarrangement of multiprotein complexes.

4 | MATERIALS AND METHODS

4.1 | mESC culture and differentiation into CMs

Strn-KO and parental wild-type (WT) mESC were kindly provided by the Haplobank cell library (https://www.haplobank.at/ecommerce/control/main) as a model for functional genomics. The details on KO mESC generation are described in Elling et al.[27] Briefly, position (chr17:78662690 genomic location in GRCm38.p2) and orientation of the mutation cassette was evaluated by reverse PCR, mapping the viral integration sites as previously described.[28] The mutation was confirmed by amplification and sequencing of the insertion site flanking region in the Strn-KO with respect to the parental WT line.[28] Both lines were initially cultured on a feeder layer of mitomycin C-treated mouse embryonic fibroblasts (Global Stem) and then adapted to feeder-free conditions in the presence of 10^3 U/mL leukemia inhibitory factor (LIF, CHEMICON International). They were maintained in ES cell complete medium (ESCM) composed of DMEM supplemented with 15% Fetal Bovine Serum (Gibco), 1% non-essential amino acids (NEAA, Gibco), 100 U/mL PenStrep (Sigma-Aldrich), 2 mM L-glutamine (Gibco), 1 mM Sodium Pyruvate (Gibco), 50 mM β-mercaptoethanol (Gibco), and LIF. For differentiation, cells were adapted to grow in feeder-free conditions; differentiation was induced by embryoid bodies (EBs) formation through the Hanging Drop technique as previously described.[29] 20 μL/500 cells drops were prepared in the differentiation medium containing: DMEM (Gibco), 1 mM sodium pyruvate, 20% FBS (Gibco), 0.1 mM NEAA (Sigma-Aldrich), 4 mM L-glutamine (Sigma-Aldrich), 0.1 mM β mercaptoethanol (Sigma-Aldrich), 100 U/mL PenStrep (Sigma-Aldrich), 20 μg/mL Ascorbic Acid (Sigma-Aldrich). Beating areas usually appear between Days 9 and 12.

4.2 | Beating area dissociation

At Days 12–15, beating areas from WT and Strn-KO lines were manually dissected under a microscope, when needed beating areas were further enzymatically dissociated into single cells as previously reported.[14] Briefly, dissected beating areas were incubated with 500 U/mL of collagenase type B (Sigma-Aldrich) in low calcium solution for 20–25 min at 37°C. The dissociation was completed by mechanical pipetting the suspension and stopped by adding fresh medium (with 20% FBS). Dissociated cells were centrifuged (at 500 rcf for 5 min), plated in differentiation medium on 0.1% gelatin-coated dishes and used after 48 h for electrophysiological recordings, Ca^{2+} dynamics, and immunofluorescence experiments.

4.3 | qRT-PCR

Total RNA was extracted by manually dissecting beating areas with RNeasy Plus Mini Kit (Qiagen) following the manufacturer's instructions. RNA concentration was measured using the NanoDrop 1000 Spectrophotometer (Thermo Scientific), while the integrity was assessed by ExperionTM Reagent SdtSens kits and Chips (Bio-Rad). RNA retro transcription was carried out using SuperScript® VILO cDNA Synthesis Master Mix (Invitrogen) in 20 μL volume. Quantitative Real-Time PCR was performed on CFX96TM Real-Time PCR (Bio-Rad), in 15 μL reaction, volume using All-in-One SYBR® Green qPCR Mix (GeneCopoeia) according to the manufacturer's instructions. Relative quantitation was performed using the

ΔΔCt method. Sequences of the used specific primers are reported in Table S1. The HPRT gene was chosen as housekeeping among three possible normalizer genes (TBP, HPRT, and GAPDH) using the NormFinder algorithm.[30]

4.4 | Western blot

Cell lysates from undifferentiated mESC and EBs of both WT and Strn-KO cell lines were obtained by using Pierce® RIPA buffer containing phosphatase (Roche) and protease inhibitors (Complete Mini Tablets, Roche). The protein concentration was determined using the Pierce® BCA (BiCinchoninic Acid) Protein Assay Kit 8 (Thermo Scientific), following the manufacturer's instructions. 15 μg of protein extracts and protein standard (Bio-Rad) were separated on NuPAGE® Novex® 4%–12% Bis-Tris Protein Gels MIDI (Thermo Scientific) and blotted on PVDF membrane, using a Criterion Electrophoresis and Blotting apparatus (Bio-Rad).

Membranes were blocked with 5% non-fat dry milk in Tris-buffered saline containing 0.1% Tween 20. Strn was detected using a mouse monoclonal anti-mouse Strn antibody (BD 6108389, 1:2000, BD Biosciences); β-actin (Sigma) was used as normalizer. Secondary HPR-conjugated goat anti-mouse antibody was used (Santa Cruz Biotechnology). Specific proteins were then visualized using the Supersignal West Dura Extended Duration Substrate detection kit (Thermo Scientific) and images captured by ChemiDoc™ Touch Imaging System (Bio-Rad).

For SERCA2a and α-tubulin, 25 μg of EBs protein extracts were separated by SDS-polyacrylamide gel electrophoresis (4%–12% Bis-Tris Criterion BIO-RAD gels), blotted for 1 h on nitrocellulose membrane and incubated overnight at 4°C with specific primary antibodies. After 1 h incubation with specific secondary antibodies labeled with fluorescent markers (Alexa Fluor or IRDye), the signal was quantified by Odyssey Infrared Imaging System (LI-COR). GAPDH was used as normalizer. Antibodies: SERCA2a anti-serum (A010-20; Badrilla), monoclonal anti α-Tubulin (Clone DM1A, Sigma-Aldrich), and anti-GAPDH (D16H11, Cell Signaling).

4.5 | Video tracking analysis

The motion of the beating areas of CMs was tracked on Day 15 of differentiation and recorded into an AVI file by the VST program (http://cismm.web.unc.edu/software/). Briefly, VST records the movements of video markers linked to beating regions of the cell cultures. By starting the videos in VST, frame by frame, the program follows and records the spatial–temporal coordinates x, y, and t for each video marker, as previously described.[8] The coordinates x and y are expressed in pixel, whereas the coordinate t is expressed in seconds.

The contraction features were calculated using a custom-made algorithm[8] written in MATLAB Programming Language (The MathWorks, Inc., Natick, MA, USA). In particular, the contraction trajectories (built with displacements, velocities and accelerations) were calculated and the mean frequency (Hz) of normal contractions was extracted (using a threshold criterion, where a contraction is identified as normal when its displacement amplitude is at least two pixels). The high-frequency noise (>10 Hz) of the movements was filtered via wavelet compression (near symmetric wavelet: Symlets 4; decomposition level: 3; compression method: global threshold leading to recover 99% of the signal energy).

4.6 | Electrophysiology

Patch–clamp measurements were performed in both WT and Strn-KO CMs isolated from beating areas at Days 12–15 of differentiation. Data acquisition was performed using either the amplifier Axopatch 200A or B, the Digidata 1200 or 1550 and the pClamp 8 or 10.0 software (Molecular Devices, LLC). Data were filtered at 1–5 kHz and sampled at 10 kHz. The analysis of the data was carried out by Clampfit 10.0 (Molecular Devices, LLC) in combination with Origin Pro 9 (OriginLab) and GraphPad Prism software 6.03 (GraphPad Software, Inc.).

Current- and Voltage-clamp recordings were performed at physiological temperature (unless otherwise specified) on single CMs enzymatically dissociated from beating areas as described above. Pipettes with resistance of 1.5–3 MΩ were used.

Spontaneous action potentials (APs) were recorded in current clamp mode in the whole cell configuration. Cells were superfused at physiological temperature (36 ± 1°C) with Tyrode's solution containing (mM): 140 NaCl, 5.4 KCl, 1.8 $CaCl_2$, 1.2 $MgCl_2$, 25 D-glucose, 5 Hepes; pH 7.4 with NaOH. Patch–clamp pipettes had resistances of 5–7 MΩ when filled with the intracellular solution containing (mM): 130 K-aspartate, 10 NaCl, 10 Hepes, 2 Na-ATP, 5 EGTA-KOH, 0.1 Na-GTP, 2 $CaCl_2$, 2 $MgCl_2$; pH 7.2 with KOH. The following parameters were analyzed: rate (Hz), the maximal slope of the AP phase 0 (dV/dt_{max}, V/s); AP amplitude (APA, mV), maximum diastolic potential (MDP, mV).

Stimulated APs were evocated in WT and Strn-KO CMs in current clamp mode at 2–8 Hz. In particular, to overcome the low expression of the inward-rectifier potassium current (I_{K1}) in mESC-CMs,[31] in silico I_{K1} was injected through the Dynamic Clamp (DC) technique

as previously reported.[32] Briefly, APs recorded from mESC-CMs, were acquired at a sampling rate of 10 kHz into the computer memory to drive the numerical I_{K1} (O'Hara-Rudy-I_{K1} model). Cell membrane capacitance (C_m) was computed in generating numerical I_{K1}; I_{K1} maximal conductance was set to 1.9 nS/μF, as required to bring diastolic potential near −80 mV, and kept constant for all experiments. During the measurements, cells were superfused at physiological temperature (36 ± 1°C) with the external solution containing (mM): 154 NaCl, 4 KCl, 2 $CaCl_2$, 1 $MgCl_2$, 5 Hepes-NaOH, 5.5 D-glucose, adjusted to pH 7.35. Patch–clamp pipette was filled with (mM): 110 K-aspartate, 23 KCl, 3 $MgCl_2$, 5 Hepes-KOH, 5 Na-ATP, 0.1 EGTA-KOH, 0.4 Na-GTP, 5 Na-phosphocreatine, 0.04 $CaCl_2$, pH 7.3 with KOH. The AP duration at 20%, 50% and 90% of the repolarization phase (APD_{20}, APD_{50}, and APD_{90}, respectively) were quantified. Beat-to-beat variability of repolarization was expressed as the short-term variability (STV) of APD_{90} (i.e., the mean orthogonal deviation from the identity line),[33,34] calculated according to Equation (1):

$$STV = \sum \left(\left| APD_{(n+1)} - APD_n \right| / \left[n_{(beats)} \times \sqrt{2} \right] \right) \quad (1)$$

for 30 consecutive APs (nbeats) at steady-state level.

The transient component of the Na^+ current (I_{Na}) was recorded as the 30 μM TTX-sensitive current at physiological temperature (36 ± 1°C). Steady-state I-V curve was obtained by applying 10 mV depolarizing steps of 100 ms from an hp of -100 mV to the range −90/+30 mV followed by a step at −20 mV. Steady-state inactivation curve was obtained from peak currents recorded at −20 mV after 100 ms preconditioning steps from −90 to +30 mV (hp −100 mV).

The late component of the Na^+ current (I_{NaL}) was recorded as the 2 μM TTX-sensitive current (I_{TTX}) during slow voltage ramps (28 mV/s) from −100 mV to +40 mV. The external and pipette solutions were the same used for stimulated APs (see above), except for EGTA concentration that was 1 mM. I_{TTX} at −20 mV was taken as representative of I_{NaL} to distinguish it from the window Na^+ current activated at more negative potentials.[11]

L-type calcium current (I_{CaL}) was recorded as the 10 μM nifedipine-sensitive current in the extracellular solution containing (mM): 135 NaCl, 1.8 $CaCl_2$, 1 $MgCl_2$, 10 CsCl, 5 Hepes, 10 D-Glucose, 0.01 TTX; pH 7.4. Intracellular solution contained (mM): 135 CsCl, 0.5 $MgCl_2$, 2 ATP-Na, 0.1 GTP-Na, 5 EGTA-KOH, 5 Hepes-KOH; pH 7.2. Steady-state I-V relationship, activation and inactivation curves were obtained by applying 10 mV voltage steps (500 ms) in the range −70 to +30 mV, followed by a step at 0 mV. Hp was kept at −50 mV to inactivate the sodium current.

To record the funny current (I_f), 1 mM $BaCl_2$ and 2 mM $MnCl_2$ were added to the Tyrode solution. I_f was activated by applying hyperpolarizing voltage steps of −10 mV to the range −35/−115 mV long enough to reach steady-state activation (hp −30 mV), followed by a fully activating step at −125 mV. Steady-state activation curve was obtained normalizing the currents measured at each test pulse to that at −125 mV.

The rapid delayed outward rectifier potassium current (I_{Kr}) was recorded in extracellular solution containing (mM): 110 NaCl, 1.8 $CaCl_2$, 0.5 $MgCl_2$, 30 KCl, 5 Hepes; pH 7.4. Steady-state I-V curve was obtained by applying a 300 ms depolarizing voltage step at +20 mV followed by 400 ms steps in the range −110/+30 mV in 10 mV increments (hp −70 mV) and a final step at −60 mV. I_{Kr} was dissected as the E4031-sensitive component (5 μM). Activation curve was obtained from tail currents at −60 mV.

To assess the expression of the Na^+/Ca^{2+} exchanger (NCX), the I_{NCX} was evaluated as the 10 mM nickel-sensitive current during voltage ramps (100 mV/s) from +60 mV to −100 mV (hp −40 mV), as previously reported, with minor modification.[35] The external solution contained (mM): 135 NaCl, 10 CsCl, 1 $CaCl_2$, 1 $MgCl_2$, 10 Hepes-NaOH, 10 TEA-Cl, 10 D-glucose, adjusted to pH 7.35 to which 0.2 mM $BaCl_2$, 0.005 mM nifedipine, 0.05 mM lidocaine, and 1 mM ouabain were added to block K^+, Ca^{2+}, Na^+ channels, and the Na^+/K^+ pump, respectively. Pipette was filled with (mM): 140 CsOH, 75 aspartic acid, 20 NaCl, 10 $CaCl_2$, 10 Hepes, 20 EGTA, 20 TEA-Cl, 5 MgATP, pH 7.3. I_{NCX} density at −80 mV and + 40 mV was taken as representative of the forward and the reverse mode working direction of NCX, respectively.

For all currents, steady-state activation and inactivation curves were fitted with the Boltzmann equation:

$$y = (1 / (1 + \exp((V - V_{1/2}) / s) \quad (2)$$

where V is voltage, y fractional activation, $V_{1/2}$ the half-activation voltage, and s the inverse-slope factor. Current densities (pA/pF) were obtained by normalizing current amplitudes to cell membrane capacitance (C_m).

4.7 | Intracellular Ca^{2+} dynamics

To estimate Strn-dependent changes in intracellular Ca^{2+} dynamics, cytosolic Ca^{2+} was recorded at physiological temperature in single V-clamped CMs loaded with Fluo4-AM (10 μM) (protocol in Figure S1). Cells were incubated for 30 min with Fluo4 at room temperature and then the dye was washed for at least 10 min to allow its de-esterification. Fluo4 was excited at 488 nm, and the emission was collected through a 530 nm band-pass filter,

converted to voltage, low-pass filtered (200 Hz) and digitized at 2 kHz after further low-pass digital filtering (FFT, 50 Hz). Cells were superfused with the external solution containing (mM): 154 NaCl, 4 KCl, 2 $CaCl_2$, 1 $MgCl_2$, 5 HEPES-NaOH, and 5.5 D-glucose, adjusted to pH 7.35 to which 1 mM $BaCl_2$ and 2 mM 4-aminopyridine were added to block K^+ channels. Patch–clamp pipettes were filled with the intracellular solution containing (mM): 23 KCl, 110 KAsp, 0.04 $CaCl_2$, 3 $MgCl_2$, 5 HEPES-KOH, 0.1 EGTA-KOH, 0.4 Na-GTP, 5 Na-ATP, 5 Na-phosphocreatine, pH 7.3, and 0.01 mM Fluo4-K^+ salt. Fluorescence at the holding potential of −80 mV was recorded to estimate the resting Ca^{2+} (Ca_{rest}). Ca^{2+} transients (CaT) were evocated at 0.5 Hz during 100 ms steps at 0 mV following 50 ms step to −35 mV to inactivate Na^+ channels and allow measurement of I_{CaL} influx.

Sarcoplasmic reticulum (SR) Ca^{2+} content (Ca_{SR}) was estimated at steady state by measuring CaT amplitude elicited by electronically timed caffeine (10 mM) pulse after 10 s at −80 mV. The caffeine-induced I_{NCX} was correlated to cytosolic Ca (Ca_i) during the final third of the caffeine-induced CaT to estimate NCX function; in particular, the slope and the x-axis intercept (Ca_{eq}) were analyzed (Figure S1).

Fluorescence was calibrated in nmol/L by estimating in each cell the maximal fluorescence (F_{max}), by increasing at the end of each experiment the intracellular Ca^{2+} concentration through a gentle patch damage. Fluorescence was converted to $[Ca]_f$ according to Equation (3)

$$[Ca]_f = F \times K_d / (F_{max} - F) \quad (3)$$

assuming a dye Ca^{2+} dissociation constant (K_d) = 400 nmol/L. Cells with $F_{max} < F$ recorded under caffeine superfusion, were not considered.

4.8 | Intracellular Na^+ levels

To estimate Strn-dependent global changes in intracellular Na^+ levels, a population analysis was performed by plating 20.000 cells/well in 96-well dark plates with transparent bottom and loading them with the Na^+-sensitive dye SBFI-AM (5 μM). Briefly, cells were incubated with the dye for 120 min in their medium at 37°C. Following dye washout, measurements were performed with FLUOstar Omega (BMG Labtech) multiplate reader, settings appropriate filters for excitation (340 nm and 380 nm) and emission (520 nm). Fluorescence (F) at both excitation wavelengths were acquired at the same time in each well every 2 s for 20 s; the mean ratio F_{340}/F_{380} was calculated offline in each well. The 96-well assay plate was maintained at 37°C for the whole experiment duration.

4.9 | Immunofluorescence

For immunofluorescence analysis, cells were plated into 4-wells chambered coverslip, and then gently washed twice with phosphate buffer saline (PBS), fixed with 4% paraformaldehyde (PFA) + 10% glycerol for 10 min at RT, washed twice with PBS and stored at 4°C until use.

Previously fixed cells were washed three times with PBS and then permeabilized with 0.1% Triton X-100 in PBS for 4 min at RT. After three washes with PBS, cells were incubated with saturating buffer (3% donkey serum, 0.3% Triton X-100 in PBS) for 30 min at RT, and then with primary antibodies diluted in 3% donkey serum, 0.3% Triton X-100 in PBS, overnight at 4°C. The following antibodies were used: anti cardiac Troponin T mouse monoclonal antibody [1C11] (1:1000; Ab8295, Abcam), anti α-tubulin chicken polyclonal antibody (1:1000; 302 206, Synaptic System), anti-tyrosinated tubulin [YL1/2] rat monoclonal antibody (1:500; ab6160, Abcam) and anti-acetyl-α-Tubulin (Lys40) (D20G3) XP® rabbit monoclonal antibody (1:200; #5335, Cell Signaling Technology). After incubation, cells were washed three times with PBS and secondary antibodies diluted in PBS 1% BSA were added and incubated for 1 h at 37°C in the dark. The following secondary antibodies were used: Alexa FluorTM 488 donkey anti-mouse (1:1000; A21202, Invitrogen), Alexa Fluor™ Plus 555 goat anti-rabbit (1:1000; A32732, Invitrogen), Alexa Fluor™ 568 donkey anti-rat (1:1000; ab175475, Abcam), Alexa Fluor® 647 donkey anti-chicken (1:300; 703-605-155, Jackson ImmunoResearch Europe LTD). After three washes with PBS, Hoechst 33342 (1:5000 in PBS; Invitrogen) was added for 15′ at RT in the dark. Finally, coverslips were mounted with Mowiol-DABCO mounting medium.

Images were acquired with spinning disk confocal microscope (Nikon), equipped with CSI–W1 confocal scanner unit, using a 100x magnification silicone-immersion objective and NIS-Element software (Nikon). For each condition, cells positive for troponin were acquired and analyzed. Z-stacks acquisitions were carried out in order to include the whole cell. Confocal images were analyzed with FiJi software (NIH) using JACoP plugin to measure colocalization and Manders' coefficients. For Manders's coefficient analyses, each single z-stack was analyzed.[36]

5 | CONCLUSIONS

In conclusion, Strn-KO significantly affects the function of mESC-CMs, modifying their electrophysiological and Ca^{2+} handling properties and producing a disorganization of the microtubule dynamics. Taken together our results indicate that Strn represents a new molecular target for

the identification of causes and potential therapies for cardiac diseases.

5.1 | Study limitations

Possible alternative experimental models to mESC could be used to study Strn role, that is human-induced pluripotent stem cells (hiPSC). It is well known that hiPSC show a phenotype comparable to ESC one[37]; however, the human environment (i.e., with hiPSC) compared with the mouse one (i.e., with mESC) is surely the best one for the translational point of view.[38] We decided to perform the study with mESC thanks to preliminary encouraging results on these cells.

mESC-derived CMs (similarly to hiPSC-derived CMs) show a quite immature phenotype compared to adult CMs[39]; however, we tried to compensate it when possible, that is by using the DC technique to overcome the low I_{K1} expression in these cells.

Finally, absolute quantitative values of calibrated intracellular Ca^{2+} levels could have been overestimated (in both experimental groups) due to uncompleted estimation of F_{max} (Equation 2) within each cell.

AUTHOR CONTRIBUTIONS

P. Benzoni: Data curation; formal analysis; methodology; writing—review & editing. **M. Arici**: Data curation; methodology; formal analysis; writing—review & editing. **F. Giannetti**: Investigation; methodology; formal analysis. **A. Cospito**: Investigation; methodology. **R. Prevostini**: Methodology. **C. Volani**: Investigation. **L. Fassina**: Investigation; formal analysis. **M. D. Rosato-Siri**: Investigation. **A. Metallo**: Formal analysis. **L. Gennaccaro**: Investigation. **S. Suffredini**: Investigation. **L. Foco**: Formal analysis. **S. Mazzetti**: Data curation; methodology. **A. Calogero**: Methodology; data curation. **G. Cappelletti**: Conceptualization; validation. **A. Leibbrandt**: Resources. **U. Elling**: Resources. **F. Broso**: Investigation. **J. M. Penninger**: Resources. **P. P. Pramstaller**: Funding acquisition. **C. Piubelli**: Investigation; conceptualization. **A. Bucchi**: Validation. **M. Baruscotti**: Validation. **A. Rossini**: Conceptualization; funding acquisition. **M. Rocchetti**: Conceptualization; project administration; writing—review & editing; writing—original draft. **A. Barbuti**: Writing—original draft; writing—review & editing.

FUNDING INFORMATION

This work was funded by the Department of Innovation, Research and University of the Autonomous Province of Bolzano, Italy, through a core funding initiative to the Eurac Institute for Biomedicine. The funding bodies had no role in the design of the study and collection, analysis, and interpretation of data and in writing the manuscript. This work was also supported by the Universities of Milano and Milano Bicocca.

CONFLICT OF INTEREST STATEMENT

The authors declare no conflict of interest.

DATA AVAILABILITY STATEMENT

The data that support the findings of this study are available from the corresponding author upon reasonable request.

ORCID

P. Benzoni https://orcid.org/0000-0002-3371-3301
M. Arici https://orcid.org/0000-0001-6509-4894
R. Prevostini https://orcid.org/0009-0005-8238-4443
L. Gennaccaro https://orcid.org/0000-0002-0438-2152
F. Broso https://orcid.org/0000-0002-1804-025X
M. Baruscotti https://orcid.org/0000-0002-6155-8388
A. Barbuti https://orcid.org/0000-0002-4521-4913

REFERENCES

1. Castets F, Bartoli M, Barnier JV, et al. A novel calmodulin-binding protein, belonging to the WD-repeat family, is localized in dendrites of a subset of CNS neurons. *J Cell Biol*. 1996;134(4):1051-1062.
2. Castets F, Rakitina T, Gaillard S, Moqrich A, Mattei MG, Monneron A. Zinedin, SG2NA, and striatin are calmodulin-binding, WD repeat proteins principally expressed in the brain. *J Biol Chem*. 2000;275(26):19970-19977.
3. Gaillard S, Bartoli M, Castets F, Monneron A. Striatin, a calmodulin-dependent scaffolding protein, directly binds caveolin-1. *FEBS Lett*. 2001;508(1):49-52.
4. Meurs KM, Mauceli E, Lahmers S, Acland GM, White SN, Lindblad-Toh K. Genome-wide association identifies a deletion in the 3′ untranslated region of striatin in a canine model of arrhythmogenic right ventricular cardiomyopathy. *Hum Genet*. 2010;128(3):315-324.
5. Meurs KM, Stern JA, Sisson DD, et al. Association of dilated cardiomyopathy with the striatin mutation genotype in boxer dogs. *J Vet Intern Med*. 2013;27(6):1437-1440.
6. Sotoodehnia N, Isaacs A, De Bakker PIW, et al. Common variants in 22 loci are associated with QRS duration and cardiac ventricular conduction. *Nat Genet*. 2010;42(12):1068-1076.
7. van der Harst P, van Setten J, Verweij N, et al. 52 genetic loci influencing myocardial mass. *J Am Coll Cardiol*. 2016;68(13):1435-1448.
8. Fassina L, di Grazia A, Naro F, Monaco L, de Angelis MGC, Magenes G. Video evaluation of the kinematics and dynamics of the beating cardiac syncytium: an alternative to the Langendorff method. *Int J Artif Organs*. 2011;34(7):546-558.
9. Huang J, Lin YC, Hileman S, Martin KH, Hull R, Yu HG. PP2 prevents isoproterenol stimulation of cardiac pacemaker activity. *J Cardiovasc Pharmacol*. 2015;65(2):193-202.
10. Derangeon M, Montnach J, Bard I, Charpentier F. Mouse models of SCN5A-related cardiac arrhythmias. *Front Physiol*. 2012;3:3. doi:10.3389/FPHYS.2012.00210
11. Rocchetti M, Sala L, Rizzetto R, et al. Ranolazine prevents INaL enhancement and blunts myocardial remodelling in a model of pulmonary hypertension. *Cardiovasc Res*. 2014;104(1):37-48.

12. Casini S, Tan HL, Demirayak I, et al. Tubulin polymerization modifies cardiac sodium channel expression and gating. *Cardiovasc Res*. 2010;85(4):691-700.
13. Kaźmierczak-Barańska J, Pęczek Ł, Przygodzka P, Cieślak MJ. Downregulation of striatin leads to hyperphosphorylation of MAP2, induces depolymerization of microtubules and inhibits proliferation of HEK293T cells. *FEBS Lett*. 2015;589(2):222-230.
14. Barbuti A, Crespi A, Capilupo D, Mazzocchi N, Baruscotti M, DiFrancesco D. Molecular composition and functional properties of f-channels in murine embryonic stem cell-derived pacemaker cells. *J Mol Cell Cardiol*. 2009;46(3):343-351.
15. Scavone A, Capilupo D, Mazzocchi N, et al. Embryonic stem cell-derived CD166+ precursors develop into fully functional sinoatrial-like cells. *Circ Res*. 2013;113(4):389-398.
16. Giannetti F, Benzoni P, Campostrini G, et al. A detailed characterization of the hyperpolarization-activated 'funny' current (if) in human-induced pluripotent stem cell (iPSC)-derived cardiomyocytes with pacemaker activity. *Pflugers Arch*. 2021;473(7):1009-1021.
17. Lei M, Jones SA, Liu J, et al. Requirement of neuronal- and cardiac-type sodium channels for murine sinoatrial node pacemaking. *J Physiol*. 2004;559(Pt 3):835-848.
18. Zaza A, Rocchetti M. The late Na+ current—origin and pathophysiological relevance. *Cardiovasc Drugs Ther*. 2013;27(1):61-68.
19. Wagner S, Dybkova N, Rasenack ECL, et al. Ca2+/calmodulin-dependent protein kinase II regulates cardiac Na+ channels. *J Clin Invest*. 2006;116(12):3127-3138.
20. Hwang J, Pallas DC. STRIPAK complexes: structure, biological function, and involvement in human diseases. *Int J Biochem Cell Biol*. 2014;47(1):118-148.
21. Guzzo RM, Salih M, Moore ED, Tuana BS. Molecular properties of cardiac tail-anchored membrane protein SLMAP are consistent with structural role in arrangement of excitation-contraction coupling apparatus. *Am J Physiol Heart Circ Physiol*. 2005;288(4):H1810-H1819. doi:10.1152/AJPHEART.01015.2004
22. Nader M, Westendorp B, Hawari O, et al. Tail-anchored membrane protein SLMAP is a novel regulator of cardiac function at the sarcoplasmic reticulum. *Am J Physiol Heart Circ Physiol*. 2012;302(5):H1138-H1145. doi:10.1152/AJPHEART.00872.2011
23. Xu Z, Schaedel L, Portran D, et al. Microtubules acquire resistance from mechanical breakage through intralumenal acetylation. *Science*. 2017;356(6335):328-332.
24. Salomon AK, Phyo SA, Okami N, et al. Desmin intermediate filaments and tubulin detyrosination stabilize growing microtubules in the cardiomyocyte. *Basic Res Cardiol*. 2022;117(1):53. doi:10.1007/S00395-022-00962-3
25. Motlagh D, Alden KJ, Russell B, García J. Sodium current modulation by a tubulin/GTP coupled process in rat neonatal cardiac myocytes. *J Physiol*. 2002;540(Pt 1):93-103.
26. Asatryan B. Cardiac Sodium Channel dysfunction and dilated cardiomyopathy: a contemporary reappraisal of pathophysiological concepts. *J Clin Med*. 2019;8(7):1029. doi:10.3390/JCM8071029
27. Elling U, Wimmer RA, Leibbrandt A, et al. A reversible haploid mouse embryonic stem cell biobank resource for functional genomics. *Nature*. 2017;550(7674):114-118.
28. Elling C, Erben P, Walz C, et al. Novel imatinib-sensitive PDGFRA-activating point mutations in hypereosinophilic syndrome induce growth factor independence and leukemia-like disease. *Blood*. 2011;117(10):2935-2943.
29. Benzoni P, Nava L, Giannetti F, et al. Dual role of miR-1 in the development and function of sinoatrial cells. *J Mol Cell Cardiol*. 2021;157:104-112.
30. Andersen CL, Jensen JL, Ørntoft TF. Normalization of real-time quantitative reverse transcription-PCR data: a model-based variance estimation approach to identify genes suited for normalization, applied to bladder and colon cancer data sets. *Cancer Res*. 2004;64(15):5245-5250.
31. Saito Y, Nakamura K, Yoshida M, et al. Enhancement of spontaneous activity by HCN4 overexpression in mouse embryonic stem cell-derived cardiomyocytes - a possible biological pacemaker. *PLoS One*. 2015;10(9):e0138193. doi:10.1371/JOURNAL.PONE.0138193
32. Rocchetti M, Sala L, Dreizehnter L, et al. Elucidating arrhythmogenic mechanisms of long-QT syndrome CALM1-F142L mutation in patient-specific induced pluripotent stem cell-derived cardiomyocytes. *Cardiovasc Res*. 2017;113(5):531-541.
33. Heijman J, Zaza A, Johnson DM, et al. Determinants of beat-to-beat variability of repolarization duration in the canine ventricular myocyte: a computational analysis. *PLoS Comput Biol*. 2013;9(8):e1003202. doi:10.1371/JOURNAL.PCBI.1003202
34. Altomare C, Bartolucci C, Sala L, et al. IKr impact on repolarization and its variability assessed by dynamic clamp. *Circ Arrhythm Electrophysiol*. 2015;8(5):1265-1275.
35. Jost N, Nagy N, Corici C, et al. ORM-10103, a novel specific inhibitor of the Na+/Ca2+ exchanger, decreases early and delayed afterdepolarizations in the canine heart. *Br J Pharmacol*. 2013;170(4):768-778.
36. Bolte S, Cordelières FP. A guided tour into subcellular colocalization analysis in light microscopy. *J Microsc*. 2006;224(Pt 3):213-232.
37. Boulting GL, Kiskinis E, Croft GF, et al. A functionally characterized test set of human induced pluripotent stem cells. *Nat Biotechnol*. 2011;29(3):279-287.
38. Jonsson MKB, Wang QD, Becker B. Impedance-based detection of beating rhythm and proarrhythmic effects of compounds on stem cell-derived cardiomyocytes. *Assay Drug Dev Technol*. 2011;9(6):589-599.
39. Shen N, Knopf A, Westendorf C, et al. Steps toward maturation of embryonic stem cell-derived cardiomyocytes by defined physical signals. *Stem Cell Reports*. 2017;9:122-135. doi:10.1016/j.stemcr.2017.04.021

SUPPORTING INFORMATION

Additional supporting information can be found online in the Supporting Information section at the end of this article.

How to cite this article: Benzoni P, Arici M, Giannetti F, et al. Striatin knock out induces a gain of function of I_{Na} and impaired Ca^{2+} handling in mESC-derived cardiomyocytes. *Acta Physiol*. 2024;00:e14160. doi:10.1111/apha.14160